# New method for determining Young's modulus by non-ideally sharp indentation

Dejun Ma
*Surface Engineering Research Institute, Chinese Mechanical Engineering Society, Beijing 100072, People's Republic of China*

Chung Wo Ong[a] and Sing Fai Wong
*Department of Applied Physics and Materials Research Center, The Hong Kong Polytechnic University, Kowloon, Hong Kong, People's Republic of China*

Jiawen He
*State Key Laboratory for Mechanical Behavior of Materials, Xi'an Jiaotong University, Xi'an 710049, People's Republic of China*

(Received 19 August 2004; accepted 9 March 2005)

In a previously developed method for estimating Young's modulus $E$ by depth-sensing indentation with spherical-tipped Berkovich indenter, the $E$ value is deduced from several functional relationships (established by finite element analysis) relating nominal hardness/reduced elastic modulus ratio ($H_n/E_r$) and elastic work/total work ratio ($W_e/W$). These relationships are specified for different absolute bluntness/maximum displacement ratios ($\Delta h/h_m$). This paper reports the generalization of the method by proposing a function to replace all the above mentioned $H_n/E_r$–$W_e/W$ relationships. The function contains only a parameter $V_r \equiv V_{ideal}/V_{blunt}$ instead of $\Delta h/h_m$, where $V_{ideal}$ is defined as the indented volume bounded by the cross-sectional areas measured at the maximum displacement $h_m$ for an ideally sharp indenter, and $V_{blunt}$ is that of the real indenter. The use of $V_r$ to replace $\Delta h/h_m$ is for the purpose of extending the application of the method for non-spherical tipped Berkovich indenters. The effectiveness of the method for materials of prominent plasticity was demonstrated by performing tests on carbon steel and aluminum alloy using three Berkovich indenters with different tip shapes.

## I. INTRODUCTION

Measurement of Young's modulus is an important subject of continuing research in the field of nanoindentation. Based on different principles, various methods have been developed. An excellent review on this topic is found elsewhere.[1] In Oliver and Pharr's (O&P's) method, assumed for elastic unloading, the reduced elastic modulus $E_r$ is expressed as[2–4]

$$E_r = \frac{\sqrt{\pi}}{2\beta}\frac{S_u}{\sqrt{A(h_{cm})}} \quad , \qquad (1)$$

where $S_u$ is the initial slope of unloading at full load $P_m$, $A(h_{cm})$ is the projected contact area measured at maximum contact depth $h_{cm}$, and $\beta$ is an indenter geometry shape factor. Young's modulus $E$ of a material is calculated from $1/E_r = (1 - \nu^2)/E + (1 - \nu_i^2)/E_i$, where $\nu$ and $\nu_i$ are the Poisson's ratios of the material and indenter, and $E_i$ is the elastic modulus of the indenter.

Another fundamental approach is based on dimensional analysis and finite element analysis (FEA).[5–7] Cheng and Cheng showed the existence of functional dependences $H/E_r = \prod_1(\sigma_y/E_r, \nu, n, \theta)$ and $1 - W_e/W = \prod_2(\sigma_y/E_r, \nu, n, \theta)$, where $H \equiv P_m/A(h_{cm})$ is hardness, $\sigma_y$ is initial yield stress, $n$ is work-hardening coefficient; $\theta$ is the half angle of a conical indenter, and $W_e$ and $W$ are the elastic work and total work equal to the areas under the unloading and loading curves. The method was developed for an ideally sharp conical indenter. A functional relationship correlating $H/E$ and $1 - W_e/W$ was derived with FEA. Through use of the measured $S_u$ and $P_m$ values, the $E_r$ value is estimated. In contrast to O&P's method, there is no need to evaluate $h_{cm}$ [or $A(h_{cm})$], such that error caused by the uncertainty in deriving $h_{cm}$ is prevented. However, the quantity $S_u$ is still needed, which may cause some uncertainty for low-load indentations where the unloading curve is quite noisy.

We also reported another method in a previous paper, based on dimensional analysis and FEA.[8] In this method,

[a]Address all correspondence to this author.
e-mail: apacwong@inet.polyu.edu.hk
DOI: 10.1557/JMR.2005.0193

 

the indented material was assumed to be an isotropic continuum medium, with rate-independent properties. When true strain $\epsilon \leqslant$ yield strain $\epsilon_y$, the true stress $\sigma$ depended linearly on $\epsilon$ in a form of $\sigma = E\epsilon$. When $\epsilon > \epsilon_y$, $\sigma$ obeyed Hollomon's power law in a form of $\sigma = \sigma_y (\epsilon/\epsilon_y)^n$. $\sigma_y = E\,\epsilon_y$ was the yield stress. The indenter was assumed to be completely elastic. The interface between the indenter and sample surface was frictionless. A nominal hardness $H_n \equiv P_m/A(h_m)$ was defined, where the denominator $A(h_m)$ was the area measured at maximum indentation depth $h_m$. Hence $H_n$ was fundamentally different from $H$. $H_n$ and the ratio $W_e/W$ are functions of $E$, $\nu$, $\sigma_y$, $n$, $E_i$, $\nu_i$, $h_m$, and an absolute bluntness $\Delta h$ as defined in Fig. 1. Further simplifications led to implicit expressions of $H_n/E_r = \Phi_H(\sigma_y/E_r, n, \Delta h/h_m)$ and $W_e/W = \Phi_W(\sigma_y/E_r, n, \Delta h/h_m)$. FEA was applied to simulate non-ideal conical indentations by varying the three independent parameters in broad ranges, which led to the establishment of seven functional relationships

$$(H_n/E_r)_j = \sum_{i=1}^{6} a_{ij}(W_e/W)^i \qquad (j = 1, 2, \ldots 7) \quad , \tag{2}$$

$a_{ij}$ are the coefficients. Each relationship was indexed by $j$, corresponding to a specific relative bluntness defined as $\Delta h/h_m$. In practical operation, $H_n$, $W_e$, and $W$ are first measured. By applying Eq. (2), seven primary values of $(E_r)_j$ values are determined, which correspond to the seven measured $\Delta h/h_m$ values respectively. An interpolation process was carried out to give an ultimate estimate of $E_r$. The method is distinctive from others because it determines $E_r$ just by referring to $H_n$, $P_m$, and $h_m$ only, which are all precisely determinable quantities in a nanoindentation test. On the other hand, it does not need the indirectly determined values $S_u$ and $h_{cm}$, so that possible errors caused by the uncertainties in determining $S_u$ and $h_{cm}$ are prevented. Moreover, the pile-up effect is treated in FEA. The tip shape effect is also considered by assuming the indenter to be sphero-conical, having the same depth dependence of cross-sectional area as a Berkovich geometry.

This paper reports the generalization of our previous method. A parameter $V_r \equiv V_{ideal}/V_{blunt}$ is introduced to replace $\Delta h/h_m$, where $V_{ideal}$ and $V_{blunt}$ are the indentation volumes generated by an ideally sharp indenter and the real indenter, respectively. The volumes are defined as those bounded by the cross-sectional areas measured at $h_m$ (Fig. 2). With the introduction of $V_r$, one may attempt to fit the expressions in Eq. (2) with a single expression containing just one variable $V_r$. This function, if it exists, is assumed to be applicable for real Berkovich indenters having arbitrary tip shapes. In this study, we concentrated on examining the applicability of the method for materials of prominent plasticity. For this purpose, analyses were made on two metal substances with the use of three Berkovich indenters with different tip shapes.

## II. GENERALIZATION OF PREVIOUS RESULTS

We recall the seven $H_n/E_r$–$W_e/W$ relationships of Eq. (2) reported in our previous study[8] for sphero-conical indenters [Figs. 5(a)–5(g) in Ref. 6]. They are replotted in Fig. 3 with different symbols and are labeled with different $\Delta h/h_m$ values equal to 0, 0.2, 0.5, 1.0, 1.5, 3.0, and 12.4. For this simple geometry (Fig. 1), the parameter $\Delta h/h_m$ satisfies the need to describe the amount of indentation (in terms of displacement) relative to the absolute indenter bluntness. However, to extend the method to cover other nonspherically tipped Berkovich indenter shapes, $\Delta h/h_m$ is no longer good enough. Instead, the $V_r$ ratio is considered to be a more suitable parameter to reflect more precisely the amount of indentation (volume) relative to that expected for an ideally sharp indenter. It is termed as the relative bluntness thereafter in this article. Through empirical numerical curve fittings, a closed-form polynomial expression containing $V_r$ only was found to exist for giving good fits to all the seven $H_n/E_r$–$W_e/W$ relationships. This function is written in the form of

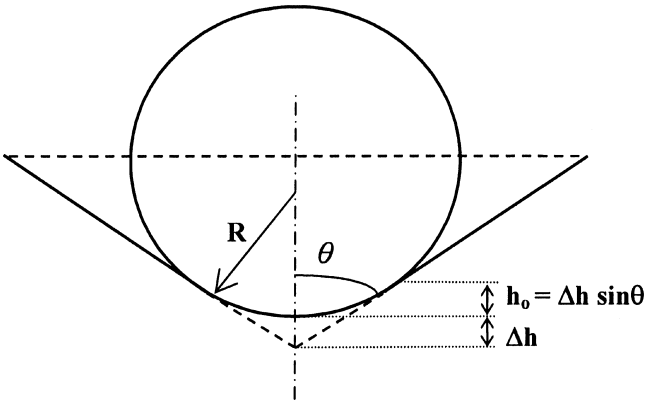


FIG. 1. Schematic presentation of a sphero-conical geometry (from Fig. 1 of Ref. 8).

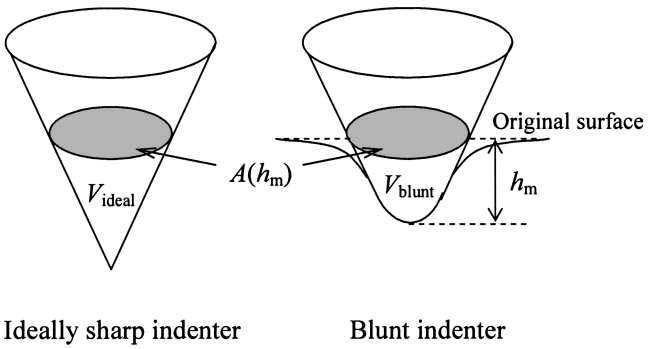


FIG. 2. Schematic presentation of an ideally sharp indenter and a blunt indenter.

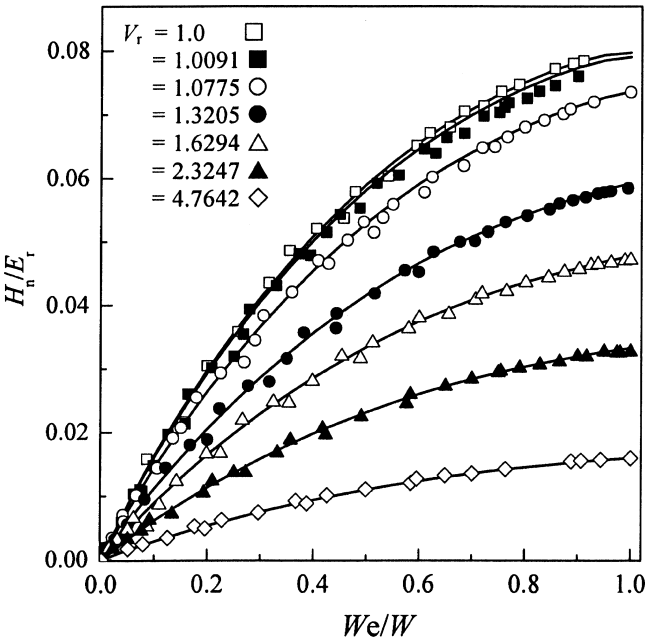


FIG. 3. Curve fittings to the seven previously established $H_n/E_r$–$W_e/W$ relationships (symbols) by substituting $V_r$ = 1, 1.0091, 1.0775, 1.3205, 1.6294, 2.3247, and 4.7642 into Eq. (3) [from Figs. 5(a)–5(g) of Ref. 8].

$$H_n/E_r = (1/V_r)\sum_{i=1}^{6} b_i\{(W_e/W)/[1 + (1.4337/V_r^3 - 0.9799/V_r^2 + 0.2517/V_r + 0.2316)(1 - 1/V_r)]\}^i \quad , \tag{3}$$

where $b_1$ = 0.18408, $b_2$ = −0.24835, $b_3$ = 0.50721, $b_4$ = −0.86118, $b_5$ = 0.75187, and $b_6$ = −0.25388. The values of $V_r$ used to substitute into Eq. (3) for producing the good fits to the $H_n/E_r$–$W_e/W$ relationships (solid curves in Fig. 3) were converted from the corresponding values of $\Delta h/h_m$ values by using the formulas given in Appendix A. Further, Eq. (3) is assumed to be applicable to any other non-ideal Berkovich indenters having an arbitrary tip shapes, although the $H_n/E_r$–$W_e/W$ relationships utilized up to now are originally developed from the assumption of sphero-conical indenter.

## III. METHOD FOR DETERMINING YOUNG'S MODULUS

Based on the establishment of Eq. (3), the previous method was generalized to provide a new approach for determining Young's modulus with non-ideal Berkovich indenters of arbitrary tip shapes. Detailed procedures are listed as follows:

(i) Calibrate the area function $A(h)$ of the Berkovich indenter used for the tests according to the tip calibration procedures proposed by Oliver and Pharr.[2,4]

(ii) Generate loading and unloading curves by making indentations on the tested material by employing a depth-sensing indentation system, and then determine the nominal hardness $H_n \equiv P_m/A(h_m)$. Further, determine $W_e$ and $W$ by integrating the areas under the unloading and loading curves, respectively.

(iii) Calculate the relative bluntness $V_r = V_{ideal}/V_{blunt}$, where $V_{ideal} = (1/3)A(h_m)[A(h_m)/24.5]^{0.5}$ for an ideal Berkovich indenter, and $V_{blunt} = \int_0^{h_m} A(h)dh$ for the real Berkovich indenter. Then evaluate the value of $H_n/E_r$ by applying Eq. (3).

(iv) Determine $E_r$ by $E_r = H_n/(H_n/E_r)$, and then $E$ of the tested material by $E = (1 - \nu^2)/[1/E_r - (1 - \nu_i^2)/E_i]$, provided that the values of $E_i$, $\nu_i$, and $\nu$ are all known.

We note that the above procedures are designed on an empirical base. In particular, the real area function of the indenter $A(h)$ evaluated at $h_m$ is used to calculate $H_n$ in step (ii), and the ideal indenter area function is used to calculate $V_{ideal}$ evaluated at that $A(h_m)$ in step (iii). The value of $V_r = V_{ideal}/V_{blunt}$ thus obtained is substitute into Eq. (3), which is responsible for making corrections for the bluntness of a real indenter. The corrections would even cover possible far field deviation of a real indenter from a standard Berkovich one. Far field deviation is reflected by having a coefficient of the $h^2$ term different from 24.5 of the standard Berkovich shape.

## IV. EXPERIMENTAL VERIFICATION OF THE METHOD

In this study, we concentrated on the use of the method on materials with strong plasticity. Two exemplified materials of this type, i.e., S45C carbon steel and 6061 aluminum alloy were selected for investigations. Two specimens of the materials were polished to produce mirror-reflecting surfaces for indentation tests. The polishing processes were performed by using grinding papers of 800, 1200, 2000, and 4000 grits, and then diamond pastes of 6, 3, 1, and 0.25 μm grain sizes. Atomic force microscopy analysis showed that the root-mean-square roughness of the polished surface was around 0.5 nm for the evaluated surface of 15 $\mu m^2$.

Three different Berkovich indenters were used for the measurements. They were installed in three nanoindenter systems (Nano Instruments, Inc., Models IIs and XP) at different laboratories (Table I). Their area functions $A(h)$ were derived according to Oliver and Pharr's procedures.[2,4] Their functional forms are summarized in Table I. Their shapes are compared with ideal Berkovich geometry with the aid of radius functions defined as $r(h) \equiv [A(h)/\pi]^{0.5}$, as shown in Fig. 4. Results show that indenter 3 is closest to the ideal one, but indenters 2 and 1 show successive increase in bluntness.

Figure 5 further illustrates how the tip geometries deviate from sphero-conical models. We created the best fits to the radius functions of the real indenters based on

TABLE I. Area functions of indenters 1, 2, and 3, installed in the systems at the Hong Kong Polytechnic University, Tsinghua University, and State Key Laboratory of Nonlinear Mechanics, Chinese Academy of Science.

| Indenter | Systems | Area function |
|---|---|---|
| 1 | Nano indenter IIs | $24.5h^2 + 1947.1030h + 7986.7031h^{1/2} + 299.6692h^{1/4} - 6373.8523h^{1/8}$ |
| 2 | Nano indenter XP | $26.2644h^2 + 1255.2840h - 1951.4068h^{1/2} - 61.7471h^{1/4} + 945.9002h^{1/8}$ |
| 3 | Nano indenter XP | $22.5984h^2 + 434.8496h - 819.8371h^{1/2} - 116.8890h^{1/4} + 83.6216h^{1/8} + 131.5329h^{1/16} + 142.0130h^{1/32} + 143.8915h^{1/64} + 143.9941h^{1/128}$ |

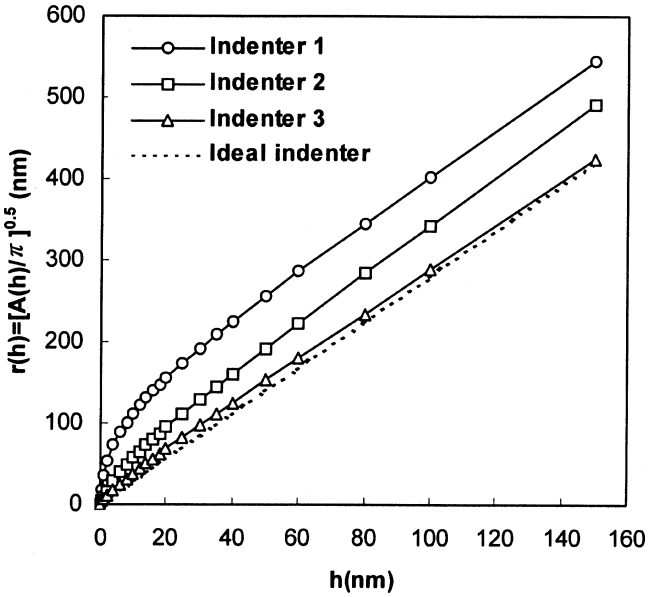


FIG. 4. Radius functions of three real Berkovich indenters and the ideal Berkovich geometry.

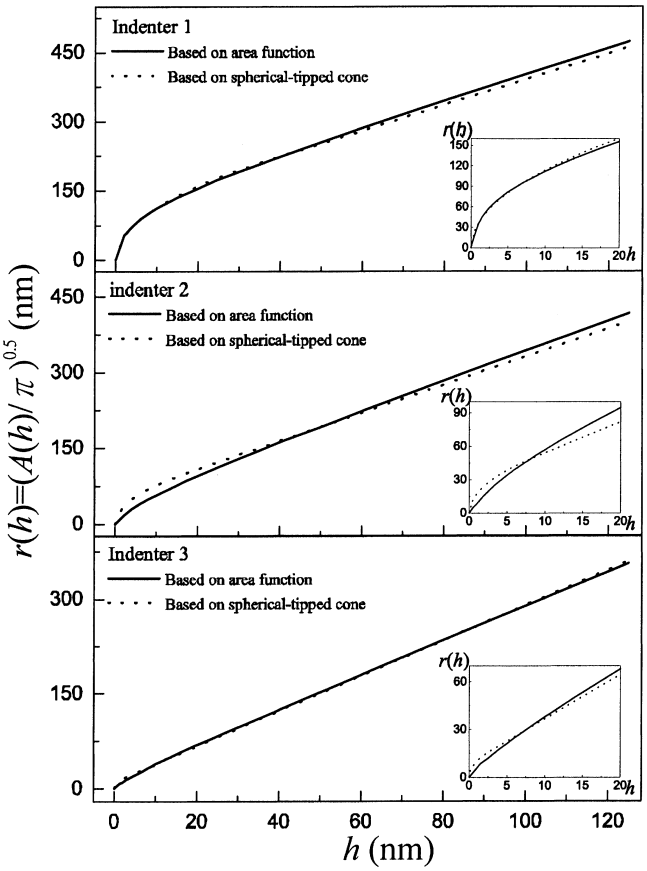


FIG. 5. Comparison between the radius functions of indenter 1, 2, and 3, and sphero-conical models of different tip radii.

sphero-conical models with different tip radii. The models were made to have a half-included angle of 70.3°, such that in the range of large $h$, the models were approximately equivalent to an ideal Berkovich indenter. Obviously, in this range of $h$, the real indenters are all dominated by the features of the ideal Berkovich geometry, and so their radius functions coincide with the best fits from the models. In the range of low $h$, rounding of the tip shapes is more pronounced. The exaggerated features for $h < 20$ nm (insets) illustrate that only indenter 1 can be described well by a spherical-tipped model (radius $R = 650$ nm). However, indenters 2 and 3 cannot be described this way; Fig. 5 shows that the area functions of indenter 2 and 3 deviate from the spherical models with $R = 225$ and 20 nm, respectively, which give the best fits to the measured results. We therefore propose that the three indenters as selected have already provided a spectrum of tip shapes for one to justify the applicability of the new method for non-ideal Berkovich indenters with different tip shapes.

Indentation tests were programmed to give different settings of full loads varying from 0.3 to 416 mN for the carbon steel and from 0.1 to 412 mN for the 6061 aluminum alloy. An indentation test consisted of approaching, loading, holding, and unloading segments. The hold segments include those conducted at maximum loads and those at the end of a test with 90% unload for thermal drift correction. Each loading, holding, or unloading segment was set to last for 50 s. Experiments of the same settings were repeated five times at different positions on a sample surface to take an average. Typical load–unload curves for S45C carbon steel and 6061 aluminum alloy for the tests of four maximum loads, produced by the three indenters, are shown in Figs. 6 and 7. Influences due to thermal drift and load frame stiffness were diminished through standard correction procedures. The $E$ values of the materials were deduced according to the procedures of the proposed method, where $E_i$ and $\nu_i$ were set to 1141 GPa and 0.07. The $\nu$ values of the carbon steel and aluminum alloy were set to 0.3 and 0.33, respectively.

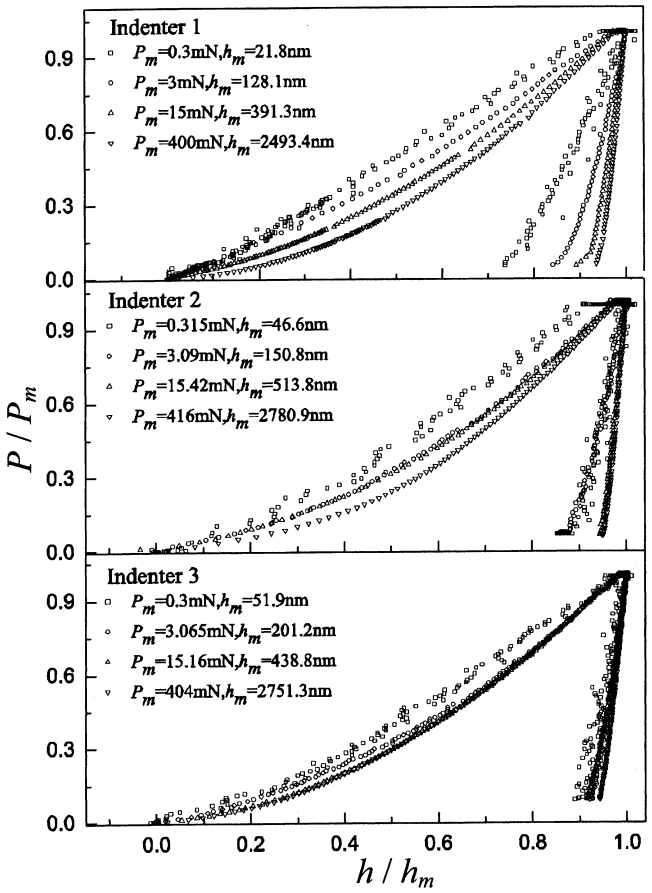


FIG. 6. Typical load–unload curves of S45C carbon steel from indentations made with four maximum loads by indenters 1, 2, and 3.

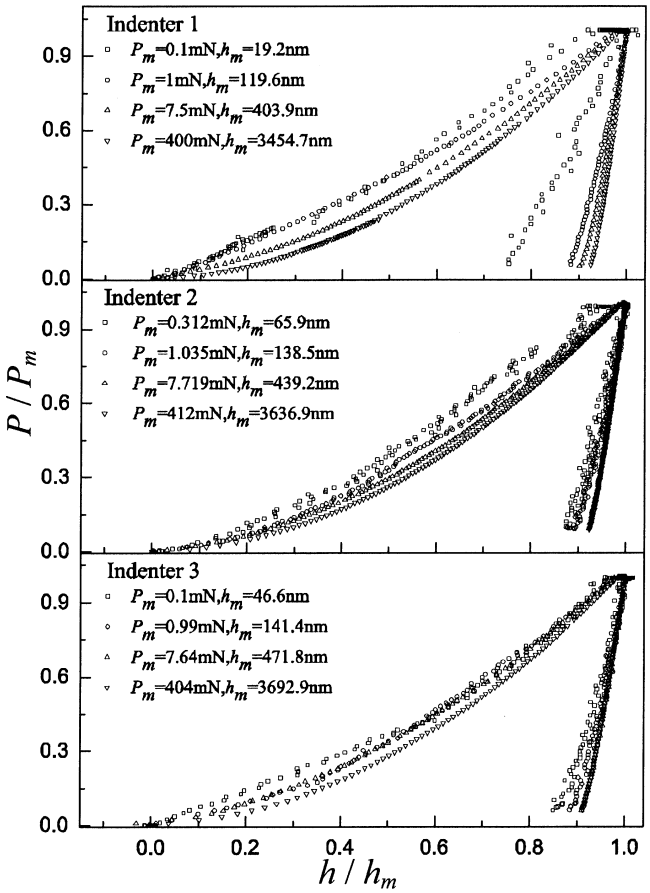


FIG. 7. Typical load–unload curves of 6061 aluminum alloy for indentations made with four maximum loads by indenters 1, 2, and 3.

To obtain references of the $E$ values for justifying the effectiveness of the new method, we performed uniaxial tensile tests for the two selected materials according to the ASTM E8M-96A standard (Standard Test Methods for Tension Testing of Metallic Materials). An MTS-810 tensile test system was used for the measurements. Results for the S45C carbon steel and 6061 aluminum alloy were 200.1 and 70.5 GPa, respectively. Dispersion of the results obtained from three identical tests falls within 2%. Considering that the samples are polycrystalline, it is possible that repetitive indentations are made on different crystallographic planes. Hence, the measured modulus values would vary in some extent, because they would be different averages of the elastic moduli of the single crystal structure. This is referred to as the anisotropic effect. According to Vlassak and Nix's results,[9–11] for a Poisson's ratio of 0.3, the indentation modulus values corresponding to different crystallographic planes of a material having an anisotropic ratio of 2.36 such as iron (Ref. 12) would not deviate from the polycrystalline indentation modulus by more than 5%. The difference is even smaller for a material having a smaller anisotropic ratio of 1.21 such as aluminum (Ref. 12). It is therefore believed that the indentation results are insensitive to the variation of grain orientation for the two materials investigated in this study and can be compared with the data obtained from macroscopic uniaxial tensile tests. As such, the tensile test results were used as standard references for the comparison of results derived from different methods of analysis.

The results of Young's modulus obtained from nanoindentation tests with various full loads and indenter shapes were normalized with respective to the results obtained from the tensile tests. The normalized $E$ values are shown in Figs. 8 and 9 and are compared with the results calculated from O&P's method using the same sets of measured data. The corresponding numerical values of $E$ for two materials are also tabulated in Tables II and III. In the table, each number for $h_m$, $V_r$ and $E$ is indeed an average of the results of five repetitive measurements, and the $\Delta E$ values represent the percentage deviations from the reference tensile test results. No results were derived from Cheng and Cheng's method[5,6] because it was for ideally sharp indentation or large indentation depth and not suitable for shallow indentation tests involved. The results of comparison show that our method gives better estimates of the Young's modulus values of S45C carbon steel and 6061 aluminum alloy,

TABLE II. Comparison of the results of S45C carbon steel obtained from the new method and Oliver & Pharr's method by using the three indenters of different tip shapes. $\Delta E = (E - 200.1)/E$. The data are the averages of the results of five measurements.

| | | Our method | | | | Oliver & Pharr's method | | |
|---|---|---|---|---|---|---|---|---|
| Indenter | Load (mN) | $h_m$ (nm) | $V_r$ | $E$ (GPa) | $\Delta E$ (%) | $h_{cm}$ (nm) | $E$ (GPa) | $\Delta E$ (%) |
| 1 | 0.30 | 22.0 | 1.740 | 210.0 ± 13 | 4.7 | 18.5 | 231.9 ± 13 | 13.7 |
| | 3.0 | 132.5 | 1.058 | 220.6 ± 13 | 9.3 | 122.7 | 273.9 ± 22 | 26.7 |
| | 15 | 387.4 | 1.003 | 212.8 ± 6 | 6.0 | 367.7 | 276.2 ± 11 | 27.6 |
| | 400 | 2511 | 0.999 | 208.5 ± 3 | 4.0 | 2424 | 278.1 ± 14 | 28.0 |
| 2 | 0.32 | 44.3 | 1.196 | 220.8 ± 16 | 9.0 | 40.7 | 214.9 ± 30 | 6.9 |
| | 3.1 | 157.3 | 1.067 | 207.7 ± 14 | 3.7 | 146.4 | 243.2 ± 11 | 17.7 |
| | 15.4 | 472.1 | 1.041 | 194.8 ± 4 | −2.7 | 452.3 | 231.5 ± 18 | 13.6 |
| | 416 | 2770 | 1.036 | 200.2 ± 4 | 0.05 | 2688 | 266.5 ± 11 | 24.9 |
| 3 | 0.30 | 47.6 | 1.010 | 217.1 ± 29 | 6.8 | 43.4 | 218.2 ± 37 | 7.1 |
| | 3.07 | 180.9 | 0.969 | 204.6 ± 11 | 2.0 | 171.1 | 273 ± 32 | 26.3 |
| | 15.2 | 455.4 | 0.963 | 192.4 ± 13 | −4.2 | 435.6 | 269.2 ± 16 | 25.4 |
| | 404 | 2696.1 | 0.961 | 172.0 ± 5 | −16.4 | 2593.4 | 226.3 ± 5 | 11.5 |

TABLE III. Comparison of the results of 6061 aluminum alloy obtained from the present method and Oliver & Pharr's method by using three indenters of different bluntnesses and tip shapes. $E$ is Young's modulus; $\Delta E = (E - 70.5)/E$. The data are the averages of the results of five measurements.

| | | Our method | | | | Oliver & Pharr's method | | |
|---|---|---|---|---|---|---|---|---|
| Indenter | Load (mN) | $h_m$ (nm) | $V_r$ | $E$ (GPa) | $\Delta E$ (%) | $h_{cm}$ (nm) | $E$ (GPa) | $\Delta E$ (%) |
| 1 | 0.10 | 19.6 | 1.831 | 71.2 ± 6.4 | 1.7 | 16.5 | 80.5 ± 11 | 11.7 |
| | 1.0 | 118.6 | 1.072 | 80.5 ± 2.7 | 12.4 | 109.6 | 91.1 ± 2.0 | 22.6 |
| | 7.5 | 413.3 | 1.002 | 79.2 ± 0.9 | 10.9 | 390.7 | 96.4 ± 2.7 | 26.8 |
| | 400 | 3469 | 1.000 | 76.8 ± 0.5 | 8.2 | 3309 | 94.4 ± 1.3 | 25.3 |
| 2 | 0.31 | 63.5 | 1.140 | 74.4 ± 5.6 | 4.3 | 57.4 | 83.7 ± 8.4 | 15.2 |
| | 1.0 | 131.2 | 1.076 | 80.6 ± 2.2 | 12.4 | 120.7 | 84.3 ± 3.6 | 16.3 |
| | 7.7 | 437.7 | 1.042 | 80.3 ± 0.8 | 12.2 | 412.8 | 86.9 ± 0.9 | 18.8 |
| | 412 | 3654 | 1.036 | 60.0 ± 0.6 | −17.5 | 3445 | 67.7 ± 0.6 | −4.1 |
| 3 | 0.10 | 43.1 | 1.016 | 68.2 ± 11.9 | −4.9 | 39.0 | 68.4 ± 13.9 | −5.3 |
| | 0.99 | 149.3 | 0.971 | 73.3 ± 7.3 | 3.3 | 139.0 | 85.7 ± 9.8 | 17.2 |
| | 7.6 | 467.6 | 0.962 | 75.3 ± 0.7 | 6.4 | 443.3 | 91.6 ± 5.2 | 22.9 |
| | 404 | 3667 | 0.960 | 63.7 ± 0.9 | −10.6 | 3476 | 78.9 ± 1.3 | 10.6 |

which are almost independent on the area functions of different Berkovich indenters used.

## V. CONSIDERATIONS OF UNCERTAINTIES AND COMPARISONS WITH OTHER METHODS

The piling-up phenomenon is an important source of uncertainty in nanoindentation tests. It is more pronounced for non-strain-hardening materials with high $E/\sigma_s$ ratios and becomes more severe with increasing load.[13] To date, there have been no adequate corrections in the O&P method for diminishing this setback. Indeed, in the O&P method, the contact area is usually underestimated when piling-up occurs and consequently gives rise to an overestimate of $E$. On the contrary, in our method, the functional relationships are generated based on FEA, and so any possible influences due to piling-up have been considered. Figures 8 and 9 show that the $E$ values determined by our method are generally lower than those of O&P's method and are closer to the reference values obtained from the tensile tests. This further justifies that the basic principle underlying the new method helps to take account of consequences due to piling-up effect, and so a more correct estimate of $E$ is obtained. We note that the present study is mainly for materials of prominent plasticity. In the next stage of out studies, investigations will be extended to cover other materials of stronger elasticity to justify the generality of the validity of the above argument.

Creep could occur in all segments in an indentation process and is supposed to be another source of uncertainty for nanoindentation tests.[14] The influence of creep is not easily evaluated quantitatively. With the use of our method based on Eq. (3), we suggest that the influences due to creep could be diminished in some extent. First, creep in the tests of full loads exceeding 0.3 mN is very mild (Figs. 6 and 7) and therefore has no need to be considered. Second, for the tests of full loads around 0.3 mN or below, some creep can be seen, such as in the holding segments. According to Eq. (3), $E_r$ scales with $1/H_n$ and $W_e/W$. When creep occurs, the unloading curve shifts toward the region of higher $h$, resulting in a higher

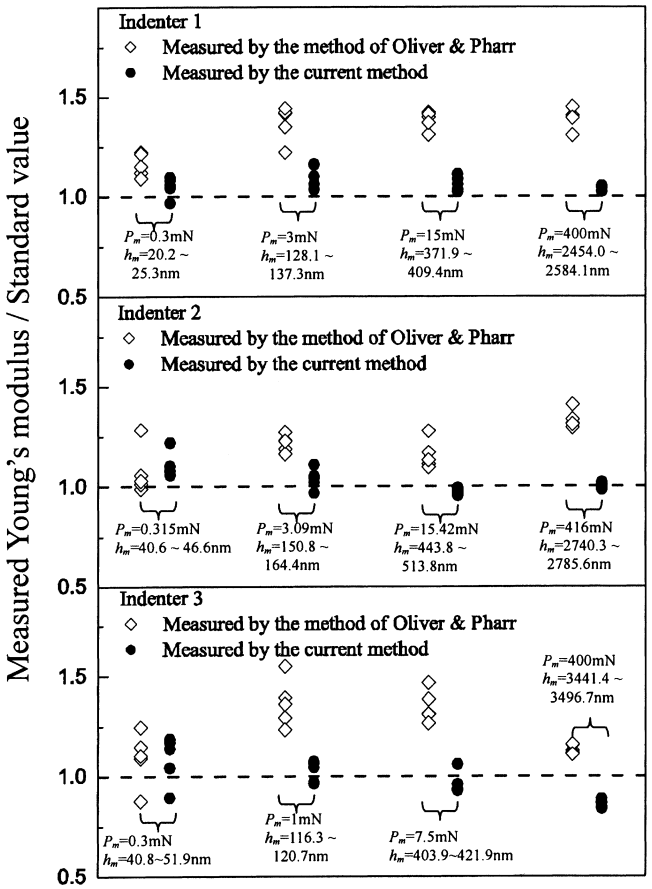


FIG. 8. Normalized Young's modulus of S45C carbon steel determined using indenters 1, 2, and 3.

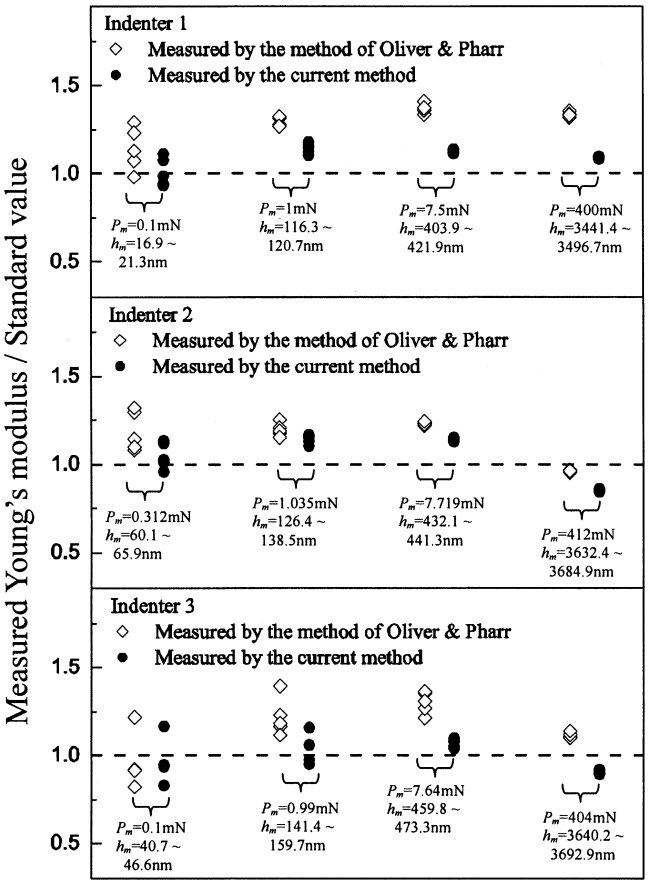


FIG. 9. Normalized Young's modulus of 6061 aluminum alloy determined using indenters 1, 2, and 3.

$h_m$ and hence a larger area $A(h_m)$. The derived value of $H_n$ would be smaller compared with the case without creep, and consequently the value of $1/H_n$ would be larger. At the same time, if the shape of the unloading curve does not change significantly but just shifts toward the higher $h$-region in a load–displacement diagram, $W$ (the area under the loading curve) becomes larger, but $W_e$ (the area under the unloading curve) is less affected so the ratio $W_e/W$ drops. Since $1/H_n$ and $W_e/W$ vary in opposite manner, this justifies our conjecture that the influence of creep on the evaluation of $E$ is reduced to some extent.

We also noticed that in a study concerning the influence of creep on the determination of Young's modulus by indentation, Chudoba and Richter[14] reported that to minimize the creep effect, the hold time must be long enough such that the depth increase in 1 min was less than 1% of total indentation depth. Referring to Chudoba and Richter's results, for materials like aluminum, a hold period of 50 s seems to serve this purpose. On the other hand, the influence of loading time is minor. In particular, referring to the load–unload curve of a test on S45C carbon steel with a maximum load of 0.3 mN (Fig. 6), the maximum depth was 21.8 nm. The average creep rate during holding was around 1 nm/50 s. At the end of holding, the instantaneous creep rate dropped to 1/5 of this value, so that in next 60 s, the further increase in depth would be around 0.24 nm, which is about 1% of the total depth. Chudoba and Richter's criterion is therefore satisfied, and the creep effect in our tests is negligible.

In general, the uncertainty of the Poisson's ratio $\nu$ of a tested material is another source of error, unless a separate experiment is carried out to determine the $\nu$ value (this is not a problem for the present demonstrative study, because the Poisson's ratios of the two selected materials are well known). Not unlike other methods, a factor in a form like $1 - \nu^2$ appears in the analysis of the presently proposed method, which contains the error caused by the uncertainty of $\nu$.[2] As a rough estimate, with the use of a reasonable guess of $\nu \sim 0.3$ with 10% uncertainty, the possible error of $E$ thus derived is supposed to be less than 3%.

To compare with other methods considered to be currently most important, the new method does not require measurement of the initial unloading slope $S_u$, contact depth, and contact area, and so any possible errors coming from the uncertainties in deriving these data can be prevented. Instead, only $h_m$, $P_m$, $W_e$, and $W$ are required

to be measured. The first two are directly accurately measurable. The latter two are obtained from integrating the areas under the unloading and loading curves and are expected to have less uncertainty compared with the process for extracting the initial unloading slope in O&P's method and Cheng and Cheng's method. This advantage is more pronounced for low-load indentations where the unloading curve is so noisy that it is not possible to derive a well-defined value of $S_u$.

## VI. CONCLUSIONS

A new method for evaluating Young's modulus by depth-sensing indentation with the use of real Berkovich indenters having arbitrary tip shapes was developed. It was generalized from a previously reported method developed by the same authors. The improved method allows the Berkovich indenter to have an arbitrary tip shape, the area function of which must be accurately calibrated at first. One assumption of the new method is that the seven $H_n/E_r$–$W_e/W$ functional relationships previously established for sphero-conical indenter are still valid for the case of nonspherical tipped Berkovich indenters. With the introduction of a volume ratio $V_{ideal}/V_{blunt}$, a single expression correlating $H_n/E_r$ and $W_e/W$ was created to replace all the seven functions. This broadens the applicability of the method for indenters having arbitrary tip shapes. In practice, by combining the measured data of $h_m$ and $P_m$ in an indentation test and the integrated areas under the load-displacement curves, the $E$ value of the indented materials can be derived from the function established. Compared with O&P's and Cheng and Cheng's methods, the new method is not subjected to the uncertainties in determining the initial unloading slope and contact depth. The applicability of the method for materials of prominent plasticity was demonstrated through tests on two example materials, i.e., S45C carbon steel and 6061 aluminum alloy. Three Berkovich indenters of different tip shapes were used for the tests to verify that the method is applicable to different tip shape. Study will be extended to materials of strong elasticity in the next stage of research to provide more sound evidence to show the applicability of the method for broader classes of substances. Finally, the single variable function is simple enough to allow a short computer program segment to be incorporated into any built-in analysis software in existing depth-sensing indentation systems, causing the proposed method to become a useful technical tool in this field of research.

## ACKNOWLEDGMENTS

The work described in this paper was substantially supported by a grant from an internal grant (Account Code: G-T 841) and another internal grant of the Hong Kong Polytechnic University.

## REFERENCES

1. A.C. Fischer-Cripps: *Nanoindentation* (Springer-Verlag, New York, NY, 2004), p. 39.
2. W.C. Oliver and G.M. Pharr: An improved technique for determining hardness and elastic modulus using load and displacement sensing indentation experiments. *J. Mater. Res.* **7,** 1564 (1992).
3. G.M. Pharr, W.C. Oliver, and F.R. Brotzen: On the generality of the relationship among contact stiffness, contact area, and elastic modulus during indentation. *J. Mater. Res.* **7,** 613 (1992).
4. W.C. Oliver and G.M. Pharr: Measurement of hardness and elastic modulus by instrumented indentation: Advances in understanding and refinements to methodology. *J. Mater. Res.* **19,** 3 (2004).
5. Y-T. Cheng, Z. Li, and C-M. Cheng: Scaling approach to modeling indentation measurements, in *Fundamentals of Nanoindentation and Nanotribology II,* edited by S.P. Baker, R.F. Cook, S.G. Corcoran, and N.R. Moody (Mater. Res. Soc. Symp. Proc. **649,** Warrendale, PA, 2001), p. Q1.1.
6. Y-T. Cheng and C-M. Cheng: Relationships between hardness, elastic modulus, and the work of indentation. *Appl. Phys. Lett.* **73,** 614 (1998).
7. C-M. Cheng and Y-T. Cheng: On the initial unloading slope in indentation of elastic-plastic solids by an indenter with an axisymmetric smooth profile. *Appl. Phys. Lett.* **71,** 2623 (1997).
8. D. Ma, C.W. Ong, and S.F. Wong: New relationship between Young's modulus and nonideally sharp indentation parameters. *J. Mater. Res.* **19,** 2144 (2004).
9. J.J. Vlassak and W.D. Nix: Measuring the elastic properties of anisotropic materials by means of indentation experiments. *J. Mech. Phys. Solids* **42,** 1223 (1994).
10. J.J. Vlassak and W.D. Nix: Indentation modulus of elastically anisotropic half spaces. *J. Mech. Phys. Solids* **67,** 1045 (1993).
11. J.J. Vlassak, M. Ciavarella, J.R. Barber, and X. Wang: The indentation modulus of elastically anisotropic materials for indenters of arbitrary shape. *J. Mech. Phys. Solids* **51,** 1701 (2003).
12. J.P. Hirth and J. Lothe: Elastic Constants, in *Theory of Dislocations* (Krieger Publishing Company, Malabar, FL, 1982), p. 837.
13. A. Bolshakov and G.M. Pharr: Influences of pileup on the measurement of mechanical properties by load and depth-sensing indentation techniques. *J. Mater. Res.* **13,** 1049 (1998).
14. Y-T. Cheng and C-M. Cheng: Scaling relationships in indentation of power-law creep solids using self-similar indenters. *Philos. Mag. Lett.* **81,** 9 (2001).
15. T. Chudoba and F. Richter: Investigation of creep behavior under load during indentation experiments and its influence on hardness and modulus results. *Surf. Coat. Technol.* **148,** 191 (2001).

## APPENDIX: RELATIONSHIP BETWEEN $\Delta H/H_M$ AND $V_{IDEAL}/V_{BLUNT}$ FOR SPHERO-CONICAL INDENTER

The ratios $\Delta h/h_m$ and $V_{ideal}/V_{blunt}$ for a sphero-conical indenter are correlated in the following two cases.

### A. In the spherical tip region $h_m \leqslant h_o$

Referring to Fig. 1, the distance between the bottom of the spherical tip, and the junction between the spherical part and conical part is defined as $h_o = \Delta h \sin\theta$. In the

spherical tip region of $h_m \leqslant h_o$, the volume $V_{blunt}$ is dominated by the spherical tip geometry, so that

$$V_{blunt} = \pi R^2 h_m - \frac{\pi}{3}[R^3 - (R - h_m)^3]$$
$$= \frac{\pi}{3} h_m{}^3 \left[ 3\left(\frac{R}{h_m}\right)^2 - \left(\frac{R}{h_m}\right)^3 + \left(\frac{R}{h_m} - 1\right)^3 \right] .$$

Considering that $R = \Delta h/(1/\sin\theta - 1)$, we obtain:

$$V_{blunt} = \frac{\pi}{3} h_m{}^3 \left[ 3\left(\frac{\Delta h/h_m}{1/\sin\theta - 1}\right)^2 - \left(\frac{\Delta h/h_m}{1/\sin\theta - 1}\right)^3 + \left(\frac{\Delta h/h_m}{1/\sin\theta - 1} - 1\right)^3 \right] .$$

On the other hand, the volume of $V_{ideal}$ can be determined as

$$V_{ideal} = \frac{\pi}{3}[R^2 - (R - h_m)^2]^{3/2}/\tan\theta$$
$$= \frac{\pi}{3\tan\theta} h_m{}^3 \left[ \left(\frac{R}{h_m}\right)^2 - \left(\frac{R}{h_m} - 1\right)^2 \right]^{3/2}$$
$$= \frac{\pi}{3\tan\theta} h_m{}^3 \left[ \left(\frac{\Delta h/h_m}{1/\sin\theta - 1}\right)^2 - \left(\frac{\Delta h/h_m}{1/\sin\theta - 1} - 1\right)^2 \right]^{3/2} .$$

From the above expressions, the ratio of $V_r$ can be expressed as

$$V_r = \frac{V_{ideal}}{V_{blunt}} = \frac{1}{\tan\theta} \frac{\left[ \left(\frac{\Delta h/h_m}{1/\sin\theta - 1}\right)^2 - \left(\frac{\Delta h/h_m}{1/\sin\theta - 1} - 1\right)^2 \right]^{3/2}}{3\left(\frac{\Delta h/h_m}{1/\sin\theta - 1}\right)^2 - \left(\frac{\Delta h/h_m}{1/\sin\theta - 1}\right)^3 + \left(\frac{\Delta h/h_m}{1/\sin\theta - 1} - 1\right)^3} .$$

### B. In the conical region $h_m > h_o$

In this region, both the spherical cap and the conical part contribute to $V_{blunt}$, so that

$$V_{blunt} = V_{Spherical\ cap} + V_{Conical\ geometry}$$
$$= \left\{ \pi R^2 h_0 - \frac{\pi}{3}[R^3 - (R - h_0)^3] \right\} + \left\{ \frac{\pi}{3}(h_m + \Delta h)^3 \tan^2\theta - \frac{\pi}{3}(h_0 + \Delta h)^3 \tan^2\theta \right\}$$
$$= \frac{\pi}{3} h_m{}^3 \left\{ 3\left(\frac{R}{h_m}\right)^2 \left(\frac{h_0}{h_m}\right) - \left(\frac{R}{h_m}\right)^3 + \left(\frac{R}{h_m} - \frac{h_0}{h_m}\right)^3 \right\} + \frac{\pi}{3} h_m{}^3 \tan^2\theta \left\{ \left(1 + \frac{\Delta h}{h_m}\right)^3 - \left(\frac{h_0}{h_m} + \frac{\Delta h}{h_m}\right)^3 \right\}$$
$$= \frac{\pi}{3} h_m{}^3 \left\{ 3\left(\frac{\Delta h/h_m}{1/\sin\theta - 1}\right)^2 (\Delta h/h_m)\sin\theta - \left(\frac{\Delta h/h_m}{1/\sin\theta - 1}\right)^3 + \left[ \frac{\Delta h/h_m}{1/\sin\theta - 1} - (\Delta h/h_m)\sin\theta \right]^3 \right\} + \frac{\pi}{3} h_m{}^3 \tan^2\theta \{ (1 + \Delta h/h_m)^3 - [(\Delta h/h_m)\sin\theta + \Delta h/h_m]^3 \} .$$

On the other hand, the volume of $V_{ideal}$ is

$$V_{ideal} = \frac{\pi}{3}(h_m + \Delta h)^3 \tan^2\theta = \frac{\pi}{3} h_m{}^3 \tan^2\theta (1 + \Delta h/h_m)^3 .$$

Therefore, the ratio of $V_r$ can be expressed as

$$V_r = \frac{V_{ideal}}{V_{blunt}} = \frac{\tan^2\theta (1 + \Delta h/h_m)^3}{\left\{ 3\frac{(\Delta h/h_m)^3 \sin\theta}{(1/\sin\theta - 1)^2} - \left(\frac{\Delta h/h_m}{1/\sin\theta - 1}\right)^3 + \left[ \frac{\Delta h/h_m}{1/\sin\theta - 1} - (\Delta h/h_m)\sin\theta \right]^3 \right\} + \tan^2\theta \{ (1 + \Delta h/h_m)^3 - [(\Delta h/h_m)\sin\theta + \Delta h/h_m]^3 \}} .$$

Obviously, for both cases $V_r$ only depends on $\Delta h/h_m$ when $\theta$ is well specified.